NJC

Accepted Manuscript

This is an *Accepted Manuscript*, which has been through the Royal Society of Chemistry peer review process and has been accepted for publication.

Accepted Manuscripts are published online shortly after acceptance, before technical editing, formatting and proof reading. Using this free service, authors can make their results available to the community, in citable form, before we publish the edited article. We will replace this *Accepted Manuscript* with the edited and formatted *Advance Article* as soon as it is available.

You can find more information about *Accepted Manuscripts* in the Information for Authors.

Please note that technical editing may introduce minor changes to the text and/or graphics, which may alter content. The journal's standard Terms & Conditions and the Ethical guidelines still apply. In no event shall the Royal Society of Chemistry be held responsible for any errors or omissions in this *Accepted Manuscript* or any consequences arising from the use of any information it contains.

ROYAL SOCIETY OF CHEMISTRY

www.rsc.org/njc

Development of nanocoral-like Cd(SSe) thin films via arrested precipitation technique and their application

Kishorkumar V. Khot[a], Sawanta S. Mali[b], Nita B. Pawar[a], Rohini R. Kharade[a], Rahul M. Mane[a], Vijay V. Kondalkar[a], Pallavi B. Patil[a], Pramod S. Patil[c], Chang K. Hong[b], Jin H. Kim[d], Jaeyeong Heo[e], and Popatrao N. Bhosale*[a].

Graphical abstract

First time synthesis of Nanoflakes to Nanocoral-like Cd(SSe) thin films, Novel Arrested Precipitation Technique, Triethanolamine as complexing agent, η=0.57%.

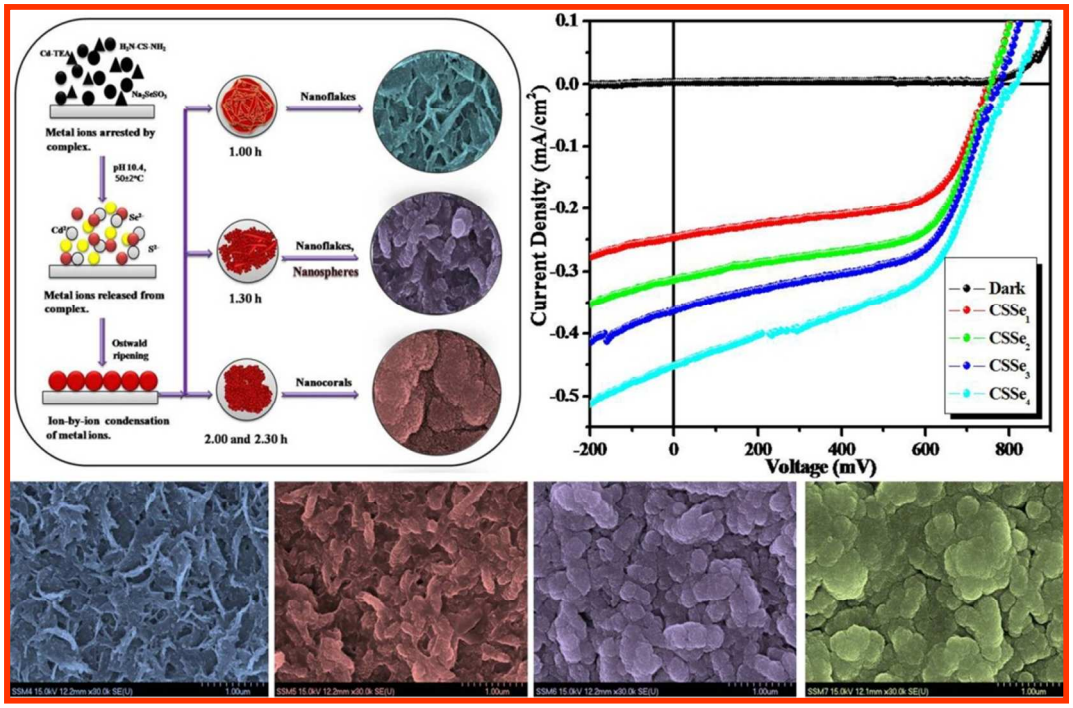

Graphical abstract: Graphical abstract of Cd(SSe) thin films.

Development of nanocoral-like Cd(SSe) thin films via arrested precipitation technique and their application

Kishorkumar V. Khot[a], Sawanta S. Mali[b], Nita B. Pawar[a], Rohini R. Kharade[a], Rahul M. Mane[a], Vijay V. Kondalkar[a], Pallavi B. Patil[a], Pramod S. Patil[c], Chang K. Hong[b], Jin H. Kim[d], Jaeyeong Heo[e], and Popatrao N. Bhosale*[a].

Graphical abstract

First time synthesis of Nanoflakes to Nanocoral-like Cd(SSe) thin films, Novel Arrested Precipitation Technique, Triethanolamine as complexing agent, η=0.57%,

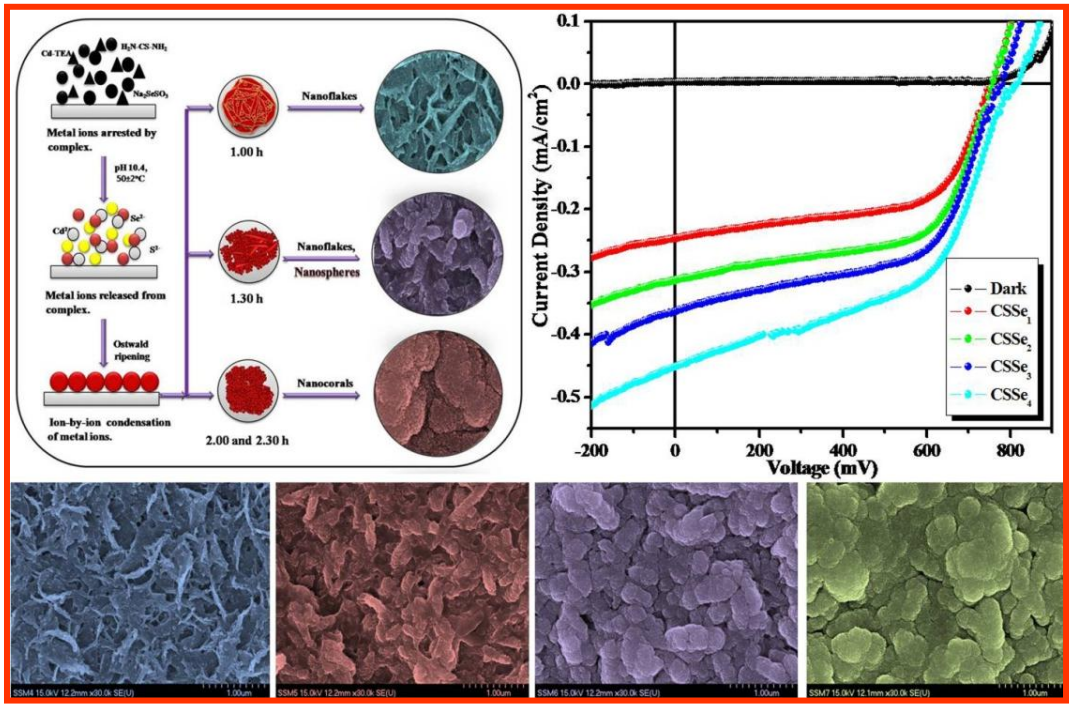

Graphical abstract: Graphical abstract of Cd(SSe) thin films.

Journal Name

RSCPublishing

ARTICLE

Development of nanocoral-like Cd(SSe) thin films via arrested precipitation technique and their application

Cite this: DOI: 10.1039/x0xx00000x

Kishorkumar V. Khot [a], Sawanta S. Mali [b], Nita B. Pawar [a], Rohini R. Kharade[a], Rahul M. Mane[a], Vijay V. Kondalkar[a], Pallavi B. Patil [a], Pramod S. Patil [c], Chang K. Hong [b], Jin H. Kim[d], Jaeyeong Heo [e], and Popatrao N. Bhosale*[a].

Received 00th January 2012,
Accepted 00th January 2012

DOI: 10.1039/x0xx00000x

www.rsc.org/

Nanocrystalline cadmium sulfoselenide thin films have been synthesized by self-organized arrested precipitation technique at different deposition time using triethanolamine as a complexing agent. Optical, structural, morphological and photoelectrochemical solar cell properties were investigated as a function of deposition time. UV-Vis-NIR absorption study suggested direct allowed type of transition and band gap energy decreased from 2.01 to 1.86 eV with increase in deposition time. X-ray diffraction studies revealed that thin films are nanocrystalline in nature with pure hexagonal crystal structure and calculated crystallite size is 51-68 nm. Field emission scanning electron microscopy demonstrated that the surface morphology was alternated from nanoflakes to assorted nanoflakes-nanospheres and finally nanocoral. X-ray photoelectron spectroscopy and energy dispersive X-ray spectroscopy showed that the composition of Cd(SSe) thin films was in good stoichiometry. Electrical conductivity and thermoelectric power measurements confirmed that the deposited films were *n*-type semiconductor. From *J-V* measurements, highest photo-conversion efficiency 0.57% was achieved. The significant boost in PEC performance might be due to the improved crystallinity with lower values of grain boundaries resistance, dislocation density and micro-strain of Cd(SSe) thin films.

Introduction

Depletion in energy sources such as, fossil fuels, coal oils, natural gas needs congregation of ever-increasing energy sources in 21st century.[1] In the last few decades, concerns about unavoidable disintegration of existing energy sources have encouraged the development of wide variety of technology to convert solar energy into electrical energy in cost-effective route. As a consequence, researchers throughout world have put their efforts to develop inexpensive and high-efficiency materials for solar cell applications. In this regards, thin film based photoelectrochemical (PEC) solar cell have wide range of application due to its cost-effective fabrication and easy junction formation with redox electrolyte.[2] Also, PEC solar cell is assumed to be a cleanest, green energy source to accomplish desired goals from the view point of photo-conversion efficiency.[3]

A broad range of II^B and VI^A group chalcogenides[4] have been synthesized and used as semiconductor nanomaterials in PEC solar cell and optoelectronic devices.[5] The main cause for their rising popularity of II^B and VI^A group chalcogenides is due to high absorption coefficient, high efficiency of radiative recombination and virtually well-matching optical band gap with visible region of solar spectrum (1.0–3.0 eV).[6] Cadmium selenide (CdSe, 1.7 eV) and cadmium sulfide (CdS, 2.4 eV) belong to II^B and VI^A group semiconductor materials. These CdSe and CdS chalcogenide thin films are mostly used as semiconducting material for CdTe/CdSe and CdTe/CdS hetero-junction photovoltaic devices[7]. They can be also act as window layers in copper indium disulfide (CIS)[8] as well as copper indium gallium sulfide (CIGS) thin film based solar cell.[9,10]

Ternary Cd(SSe) thin films can be synthesized by a variety of techniques, such as, chemical bath deposition,[11-13] evaporation,[14-17] solvothermal route,[18] sputtering[19] and chemical spray pyrolysis.[20] On the contrary, these methods demand harsh experimental condition, toxic reducing agent, organic surface directing agents, solvents and highly sophisticated instruments. In the present effort, arrested precipitation technique (APT) was used for deposition of high-quality Cd(SSe) (abbreviated as CSSe) thin films. APT is a self-organized, cost effective, suitable for large area deposition, and it does not require sophisticated instruments.[21-22] In addition, APT is a hybrid chemical method of chemical bath deposition (CBD) technique in combination with controlled chemical growth process (CCGP).[23-24] CSSe thin films as a semiconducting materials has been applied in various fields including PEC solar cell, wavelength-tunable nano-optoelectronic devices,[25] and phototransistors.[26] Taking into consideration the significant advantages laid down by ternary CSSe thin films, we have synthesized ternary CSSe thin films by using APT. Recently, we have successfully synthesized novel ternary and quaternary mixed metal chalcogenides thin films such as, $MoBi_2S_5$,[23] $Mo(S,Se)_2$,[27] $Bi_2(S,Se)_3$[28] and $MoBiGaSe_5$,[23] $MoBi_2(Se,Te)_5$,[24] $MoBiInSe_5$[21] by using APT for PEC solar cell and thermocooling applications.

To the best of our knowledge, there is no particular report available on novel synthesis of nanocoral-like CSSe thin films

using APT. Most of complexing agents being used are flammable, carcinogenic and toxic in nature.[29,30] We have selected triethanolamine (TEA) as a stable complexing agent. The intention of this report is to optimise growth pathway and engineer surface morphology of CSSe thin films using TEA as complexing agent. Moreover, we have demonstrated PEC performance with highest conversion efficiency 0.57%. Also, comprehensive growth mechanism for formation of CSSe thin films was discussed.

2 Experimental

2.1 Materials and method

All chemicals were of analytical reagent (AR) grade and used without further purification. Cadmium sulfate hydrate ($CdSO_4 \cdot H_2O$) (98%, S-D Fine Chem.), thiourea (H_2N-CS-NH_2) (99%, S-D Fine Chem.) selenium metal powder (99.5%, Sigma Aldrich), sodium sulfite (Na_2SO_3) (96%, S-D Fine Chem.), liquor ammonia (NH_3) (28-30% Thomas Baker), and triethanolamine ($N(CH_2\text{-}CH_2\text{-}OH)_3$) (99%, Merck) were used as precursors and complexing agent. For measurement of photoelectrochemical cell properties we have used sulfide/polysulfide redox electrolyte prepared from sodium sulfide (Na_2S) (Thomas Baker), sodium hydroxide pellets (NaOH) (99%, S-D Fine Chem.) and sulfur powder (99%, S-D Fine Chem.). The substrates were ultrasonically cleaned using detergent followed by methanol treatment and finally cleaned with acetone and deionized water. Herein, CSSe thin films were deposited onto bare as well as ITO-coated glass substrates (sheet resistance 20-25 Ω cm^{-2}) by using simple APT.

2.2 Deposition of CSSe thin films

In typical synthesis Cd-TEA complex react with S^{2-}, and Se^{2-} chalcogen ions, which are released slowly from dissociation of H_2N-CS-NH_2 and Na_2SeSO_3 at alkaline pH 10.4 and 50±2ºC temperature. Solution of 0.05 M Cd-TEA complex was used as a source for Cd^{2+} ions, where cadmium sulfate was triturated with TEA as complexing agent for 6 h to form clear solution of Cd-TEA complex. Sodium selenosulfite (Na_2SeSO_3) was prepared by refluxing selenium metal powder with anhydrous sodium sulfite at 90°C for 8 h.

Nucleation and thin film formation is mainly dependant on different preparative parameters such as, complexing agent, precursor concentration, pH, deposition time and temperature of bath. These parameters were optimized during the initiative stage of thin film deposition. All precursors' concentration was kept constant as 0.05 M and deposition time was varied from 1.00, 1.30, 2.00, and 2.30 h. After each interval of deposition time, film thickness was checked by surface profiler. It was seen that at the terminal growth of films, film thickness remains constant after 2.30 h. At the same time, peeling of substrate with irregular grown surface without increase in film thickness was observed with further increase in deposition time. So, we have studied effect of deposition time up to 2.30 h. Effect of deposition time on thickness of thin films is explained in detail in electronic supplementary information. At the terminal growth phase all the deposited thin films were dark orange-red in colour and well adherent to substrate surface. The deposited films were correspondingly designated as, $CSSe_1$, $CSSe_2$, $CSSe_3$ and $CSSe_4$ respectively. The optimized preparative parameters were tabulated in Table 1.

2.3 Characterization of thin films

Thickness of deposited thin films was measured by using surface profiler (AMBIOS XP-1). Optical absorption spectra were recorded using UV-Vis-NIR spectrophotometer (Shimadzu, UV-1800). Structural properties were confirmed by using X-ray diffractometer (Bruker AXS, D8) using Cu Kα (λ =1.5418 Å) radiation for 2θ ranging from 20º to 80º. Surface morphology and elemental composition of as-deposited thin films were investigated using field-emission scanning electron microscopy (FESEM) equipped with energy dispersive X-ray spectroscopy (EDS) analyzer (Hitachi, S-4700). Elemental information concerning to as-deposited CSSe thin films was characterized by using an X-ray photoelectron spectrometer (XPS, Thermo Scientific, Multilab-2000) with a multi-channel detector, which can endure high photon energies from 0.1-3.0 KeV. Electrical conductivity (EC) was measured by using two probe method. Thermoelectric power (TEP) measurements were conducted under condition of maximum temperature difference and minimum contact resistance using C-T meter apparatus (Teleph-France). PEC measurements were carried out using semiconductor parameter analyzer (Keithley SCS-4200 Semiconductor) characterization unit in dark and under illumination using 500 W tungsten filament lamp (Intensity 30 mW/cm^2) in sulfide/polysulfide redox electrolyte. PEC cell was fabricated using standard two-electrode configuration, comprising glass-ITO/Cd(SSe) (active surface area of 1 cm^2) photoelectrode, and graphite as counter electrode. All measurements were done at room temperature (300K) in air.

3 Results and discussion

3.1 Growth and reaction mechanism of thin film formation

In arrested precipitation metal ions are arrested by using TEA as complexing agent and are released at optimized precursor concentration, pH and temperature. Aqueous ammonia used to optimize pH, which is source to increase the concentration of OH^- ions, relative molecular area and solubility of S^{2-}, Se^{2-} chalcogen ions in reaction solution.[31] Generally, at higher temperature large number of metal ions are released and reaction rate gets faster which causes bulk precipitation rather than desired thin film formation.[32] So at initiative stage, we have optimised deposition temperature, precursor's concentration and pH as 50±2ºC, 0.05 M and 10.4 respectively to achieve high-quality, pin-hole free CSSe thin films. APT is based on Ostwald ripening law.[32] According to this law, rate of reaction between metal ions along with chalcogen ions can be controlled by using stable complexing agents (in our case TEA).

Table.1 Preparative parameters for synthesis of CSSe thin films, pH= 10.4, Temperature= 50±2ºC, rpm (rotation per minute)= 45.

Sr. No.	Sample Code	Deposition Time (h)
1	$CSSe_1$	1.00
2	$CSSe_2$	1.30
3	$CSSe_3$	2.00
4	$CSSe_4$	2.30

Smaller nucleus or embryos come towards each other to form less stable crystals which readily convert into large crystal. As deposition time increases the additional metal ions will be released, which cause dissolution of smaller particles and formation of well grown stable large crystals. Formation of thin film occurs, when

ionic product (Kp) exceeds the solubility product (Ksp) of metal ions and multi-nucleation process next to ion-by-ion condensation of metal ions onto the substrate surface.[21] When all metal ions and chalcogen ions in solution vanishes with increase in deposition time films thickness terminates, called as terminal thickness of deposited thin films.[24] Generally, slow reaction rate results in formation of good-quality and adherent thin films.[21] Hence, developed arrested precipitation technique is effective as compared with routine chemical bath processes. Comprehensive growth mechanism for the formation of CSSe thin films is exposed in scheme 1.

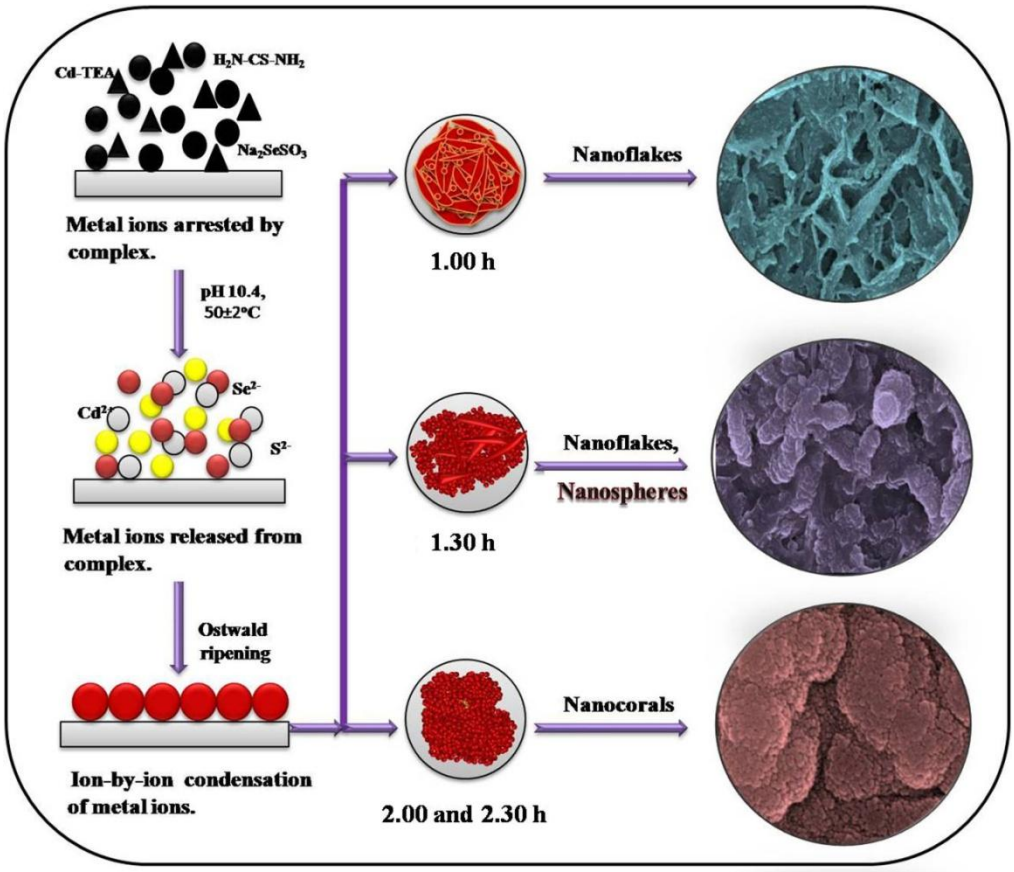

Scheme 1 Comprehensive growth mechanism of CSSe thin films.

Plausible reaction pathway of cadmium sulfoselenide thin films is summarized as follows,

Initially, Cd^{2+} ions are released from the dissociation of Cd-TEA metal complex as shown in reaction 1.

$$(NH_4)_4[Cd2N(CH_2\text{-}CH_2\text{-}O)_3] + 6H_2O \xrightarrow[T= 50°C\pm0.5]{pH\ 10.4} Cd^{2+} + [2N(CH_2\text{-}CH_2\text{-}OH)_3] + 4NH_4OH + 2OH^- \quad (1)$$

Further at alkaline pH sodium selenosulfite dissociates into sodium sulfate and highly active HSe^- species. This highly active species quickly converts into Se^{2-} ions (reactions 2 and 3).

$$Na_2SeSO_3 + OH^- \xrightarrow{pH\ 10.4} Na_2SO_4 + HSe^- \quad (2)$$

$$HSe^- + OH^- \longrightarrow H_2O + Se^{2-} \quad (3)$$

At the same time thiourea dissociate to release S^{2-} ions as shown in reactions 4 and 5,

$$H_2N\text{-}\overset{\overset{S}{\|}}{C}\text{-}NH_2 + OH^- \xrightarrow{pH\ 10.4} H\,S^- + H_2N\text{-}\overset{\overset{O}{\|}}{C}\text{-}NH_2 \quad (4)$$

$$HS^- + OH^- \longrightarrow S^{2-} + H_2O \quad (5)$$

When the ionic product of Cd^{2+}, S^{2-} and Se^{2-} ions exceed solubility product of Cd(SSe) in reaction bath, which results in slow ion-by-ion condensation of metal ions and chalcogen ions on the basis of Ostwald ripening law.

$$Cd^{2+} + 1/2\ S^{2-} + 1/2\ Se^{2-} \xrightarrow[T= 50°C\pm2]{pH\ 10.4} Cd(SSe) \quad (6)$$

3.2 Optical absorption studies

Fig.1(a) shows optical absorption spectra of CSSe thin films recorded using UV-Vis-NIR spectrophotometer in wavelength range 350-1100 nm. Fig.1(a) clearly shows that maximum optical absorption is observed at around 650-750 nm. The enhancement in absorption spectra is due to considerably improvement in crystallinity for all CSSe thin films. Absorption coefficient for all samples is found to be in order of 10^5 to10^6 $cm^{-1.}$ The fundamental absorption, which corresponds to electron excitation from the valance band to conduction band, can used to determine value of optical band gap energy. Optical data were demonstrated by using following equation 7; [33]

$$\alpha = \frac{A(h\vartheta - Eg)^n}{h\vartheta} \quad (7)$$

where, 'A' is a parameter depends on transition probability, *h* is Planck constant, *'E_g'* is the optical band gap energy of material, and exponent '*n*' depends on type of transition. The values of *'n'* for direct allowed, indirect allowed, direct forbidden and indirect forbidden transition are 1/2, 2, 3/2 and 3, respectively.

Table 2 Statistics of the thickness, optical band gap (*Eg*), crystallite size (D), dislocation density (δ) and micro-strain (ε) of Cd(SSe) thin films.

Sample Code	Thickness (nm)	Band Gap (eV)	Crystallite Size (nm)	Dislocation Density (δ) 10^{-4} lines m^{-2}	Micro-strain (ε) 10^{-4}(lines^{-2} m^{-4})
$CSSe_1$	535	2.01	51	3.8	7.0
$CSSe_2$	603	1.95	57	3.0	6.2
$CSSe_3$	720	1.90	63	2.5	5.6
$CSSe_4$	793	1.86	68	2.16	5.2

Optical band gap energy values of CSSe thin films were obtained by plotting graph of $(\alpha h\vartheta)^2$ *vs.* photon energy ($h\vartheta$), as shown in Fig 1(b). Linear nature of plot suggests direct and allowed type of transition. The band gap energy is decreased from 2.10-1.86 eV with increase in deposition time. The optical band gap values are in well agreement with reported values.[10] These obtained band gap energies are summarized in Table 2. From optical absorption study, it revealed that optical absorption shifted towards red shift region and decrease in optical band gap energies is due to increase in thickness of CSSe thin films with increase in deposition time (1.00-2.30h).

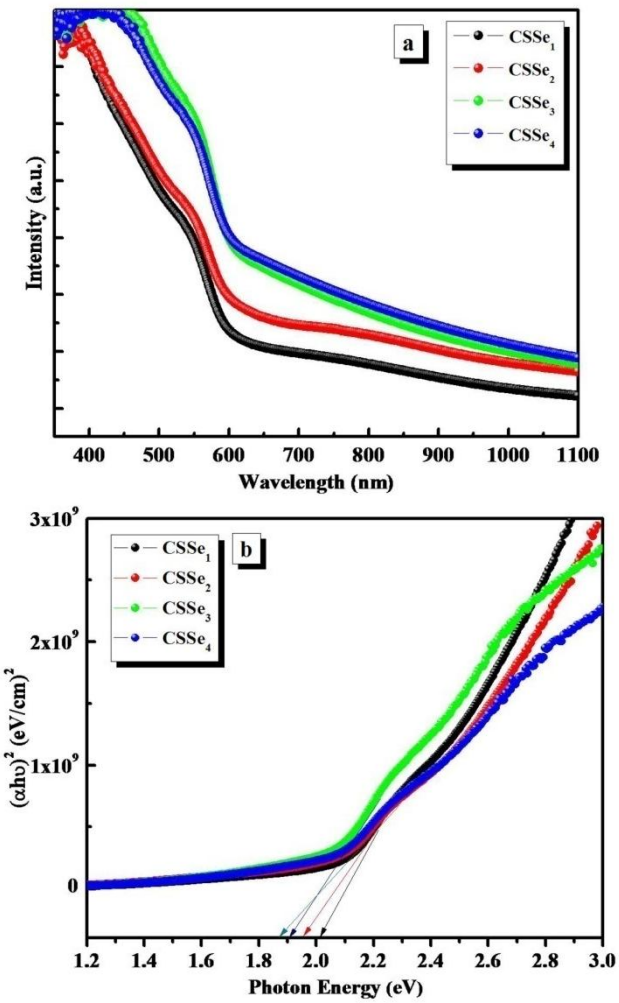

Fig.1(a) Optical absorption spectra of CSSe thin films, **(b)** Plots of $(\alpha h\upsilon)^2$ $(eV/cm)^2$ vs. photon energy (eV).

3.3 Structural studies

Crystal quality and structural analysis was carried out by using X-ray diffraction pattern in range of 20º to 80º. Fig. 2 shows X-ray diffraction patterns of CSSe thin films. The broad and intense peaks in XRD pattern confirm that all samples are nanocrystalline in nature.[21] The major diffraction peaks centred at 2θ 26.10º, 30.43º, 31.50º, 42.30º, 43.40º, 50.06º and 51.97º can be indexed to (002), (101), (102), (110), (103), (200) and (201) crystal planes, respectively. The XRD patterns show major intense peak at 2θ = 26.10º (002). The experimental d-values are in well agreement with standard d-values (*JCPDS* card no. 49-1459) for an (*hkl*) plane confirms formation of CSSe thin films with pure hexagonal crystal structure. Values of 2θ, respective (*hkl*) planes, corresponding experimental and *JCPDS* d-values are summarized in Table 3. Last column of Table 3 shows differences between experimental and standard d-values determined from relation, Δd (Å) = $d(Å)_{Exp}$ - $d(Å)_{JCPDS.}$ In typical X-ray diffraction patterns of CSSe thin films, all peaks occur at identical positions with amendment in intensity and boarding of diffraction peaks, which ensures that creation of pure phase material and improvement in crystal quality with increase in deposition time. Also, no any other peaks are observed, reveals that material is in pure phase. The observed boarding of diffraction peak may be due to strain or micro-strain.[34,35] Further, average crystallite size was calculated by using Scherrer formula (equation 8),[36,37]

$$D = \frac{0.94\lambda}{\beta \cos\theta} \qquad (8)$$

where, D is crystallite size, λ is wavelength of X-ray radiation (1.5406 Å), β the full-width-at-half-maximum (FWHM) in radian, and θ is Bragg's angle. Calculated crystallite size is from 51 to 68 nm with increase in deposition time. These enhancement in crystallite size with minimum interfacial energy is beneficial for improvement of photon conversion efficiency.[38,39] From calculated crystallite size (D), dislocation density (δ) and micro strain (ε) for all samples were determined by using equations 9 and 10 and are summarized in Table 2;

Table3 X-ray parameters of the CSSe thin films.

Sr. No.	2θ	(*hkl*)	d (Å)$_{Exp.}$	d (Å) $_{JCPDS.}$	Δ d (Å)
1	26.10	002	3.412	3.389	0.023
2	30.43	101	3.335	3.185	0.150
3	31.50	102	2.537	2.470	0.067
4	42.30	110	2.134	2.088	0.046
5	43.40	103	2.082	1.921	0.161
6	50.06	200	1.820	1.800	0.020
7	51.97	201	1.757	1.750	0.007

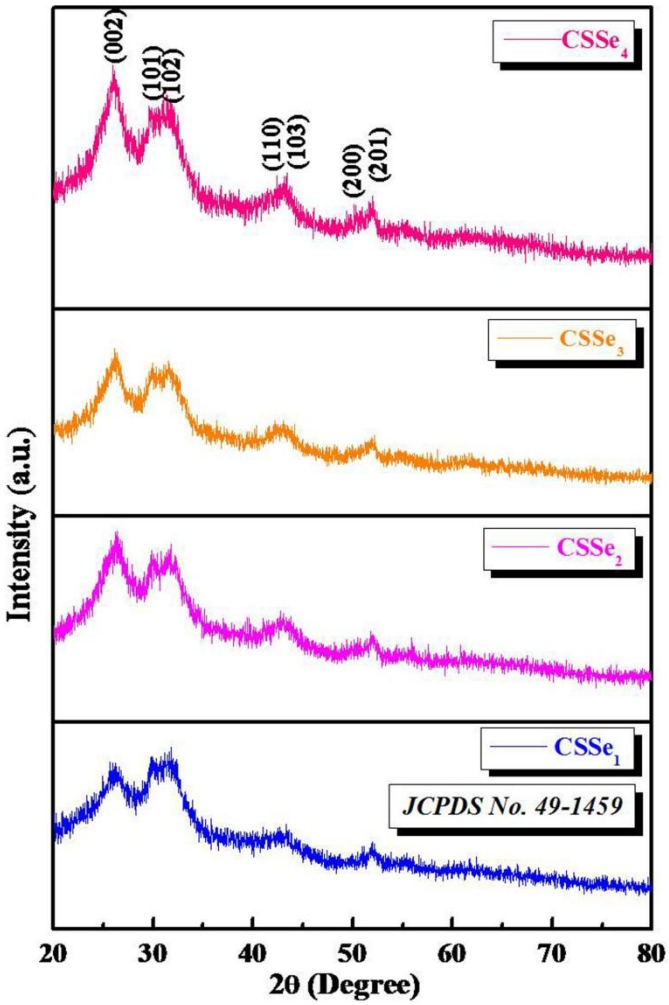

Fig. 2 X-ray diffraction patterns of CSSe thin films.

$$\delta = \left(\frac{1}{D^2}\right) \qquad (9)$$

$$\varepsilon = \left(\frac{\beta \cos\theta}{4}\right) \qquad (10)$$

The lower values of δ and ε are noted for all samples with increase in deposition time. This is endorsed to decrease in defect levels and grain boundaries due to enhancement in crystallite size.[40,41]

Decrease in δ and ε indicates lower level of lattice imperfections[42-44] and formation of high-quality CSSe thin films with increase in deposition time. The lattice parameters for hexagonal crystal structure (a=b≠c) were calculated by using following equation 11,

$$\frac{1}{d} = \frac{4}{3}\left(\frac{h^2 + hk + k^2}{a^2}\right) + \frac{l^2}{c^2} \qquad (11)$$

The lattice parameters were found to be a = b = 4.2595Å and c = 6.8410Å. These lattice parameters are in good agreement with standard *JCPDS* data (49-1459). Increase in crystallite size was

correlated to decrease in band gap with increase in deposition time.[45,46]

3.4 Morphological studies

Surface morphology and composition of deposited CSSe thin films were characterized by using FESEM and EDS. Fig.3 show FESEM micrographs of CSSe thin films at low and high magnifications with increase in deposition time. FESEM micrographs show that uniform, well-adherent, pin-hole free thin films deposition over entire substrate surface. Fig.3(a,b) show FESEM images for CSSe thin films deposited at 1.00 h deposition time. The beaded nanoflake-like morphology is evident from low magnification image (Fig.3(a)). From Fig.3(b), it is observed that numerous grown nanoflakes over entire substrate surface are interconnected to each other. These nanoflakes have average thickness of ~80 nm. Fig. 3(c,d) show FESEM images for CSSe thin films deposited at 1.30 h deposition time. The construction of assorted nanoflakes-nanospheres morphology is indicated from Fig.3(c). From higher magnification image (Fig.3(d)) assorted nanoflakes-nanospheres have average thickness ~50 nm. Decrease in thickness is might be due to construction and aggregation of assorted naoflakes-nanospheres with increase in deposition time. Fig. 3(e,f) shows FESEM images for CSSe thin films deposited at 2.00 h. Complete conversion of assorted nanflakes-nanospheres to nanocoral-like morphology is observed from Fig.3(e). From higher magnification image (Fig.3(f)), it clearly shows that single nanocoral have average ~220 nm size. Fig.3(g,h) shows FESEM images for CSSe thin films deposited at 2.30 h deposition time. Formation of large sized nanocorals due to aggregation of small sized nanocorals is observed from Fig.3(g). From Fig.3(h), it is seen that aggregated nanocorals are of ~400 nm size. FESEM micrographs signify that evolution of morphology from interconnected nanoflakes to assorted nanoflakes-nanospheres and finally nanocoral-like morphology.

Formation of nanocoral-like morphology is demonstrated in Scheme 2. Formation of such nanocoral-like morphology is observed through assembling large number of small nanosphere. These small nanospheres are interconnected to each other which lead to formation of nanocorals. The right side of Scheme 2 shows artifact of nubbly-like texture. Nubbly-like texture is nothing but irregularly grown surface. It is evident from Scheme 2 that the nubbly-like texture is reflected in nanocoral-like morphology as shown in left side of figure. This nanocoral-like morphology is favourable for absorption of large amount of solar radiation, because of its high surface to volume ratio.[47]

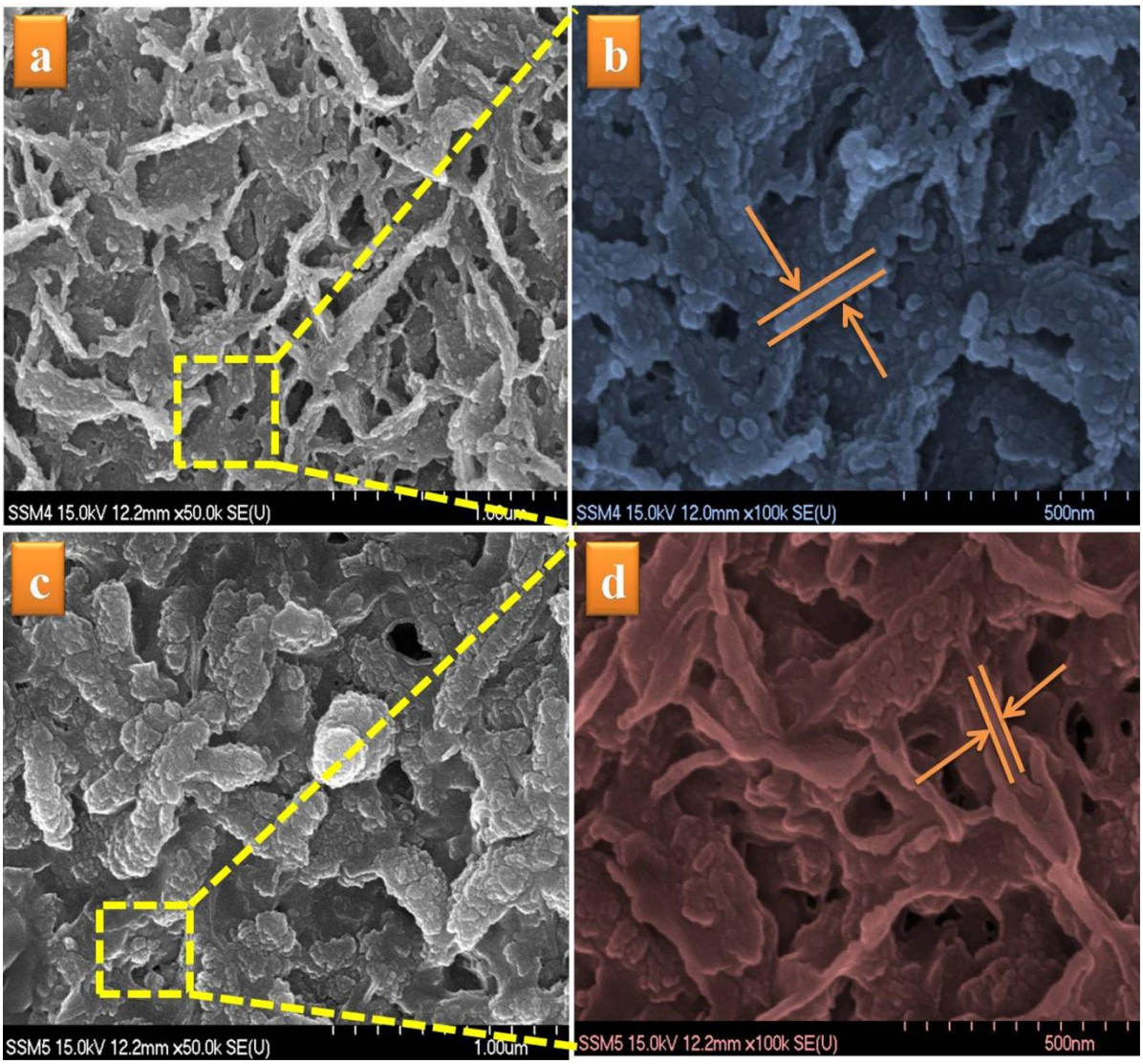

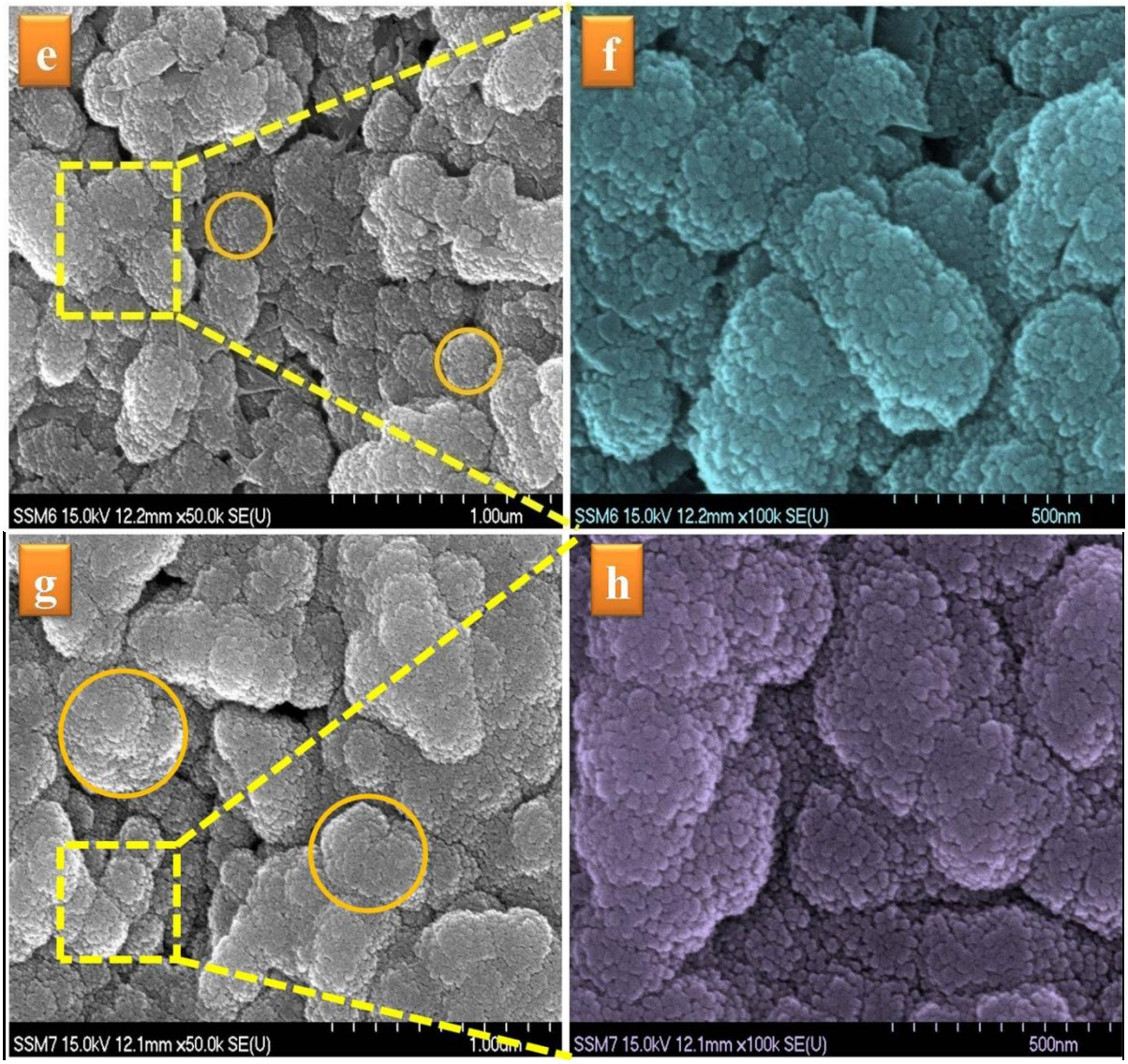

Fig. 3 Field emission scanning electron microscopy (FESEM) micrographs of CSSe thin films deposited at various deposition times, **3(a, b)** 1.00h, **3(c, d)** 1.30h, **3(e, f)** 2.00h, **3(g, h)** 2.30h,respectively.

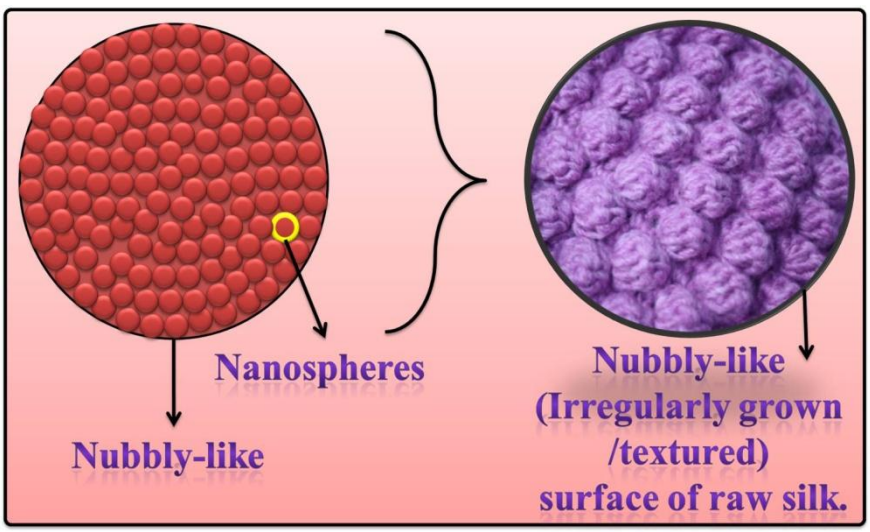

Scheme 2 Schematic representation of formation of nanocoral (Nubbly-like) morphology.

3.5 Compositional analysis

XPS analysis was carried out to determine surface composition of $CSSe_4$ thin film, as shown in Fig.4. Typical XPS survey spectrum (Fig.4(a)) of $CSSe_4$ thin film indicates the presence of cadmium (Cd), sulfur (S), selenium (Se), carbon (C), and oxygen (O) elements. The binding energies recorded in the XPS analysis were corrected to take into account specimen charging by setting C 1s at 285.02 eV. High resolution core level spectrum for Cd(3d) is shown in Fig.4(b). The two peaks in Cd(3d) core level spectrum arise with $Cd3d_{5/2}$ peak position at 405.03 eV and $Cd3d_{3/2}$ at 412.18 eV binding energies respectively. S(2p) spectrum (Fig.4(c)) shows two relevant peaks for $S2p_{3/2}$ at 160.5 eV and $S2p_{1/2}$ at 161.7 eV binding energies respectively. High-resolution core level spectrum for Se(3d) depicted in Fig.4(d). Core level spectrum for Se(3d) was fitted using single peak for binding energy at 54.10 eV. The values of binding energies for Cd, S and Se are at their respective positions for Cd^{2+}, S^{2-} and Se^{2-} states. It means that Cd^{2+}, S^{2-} and Se^{2-} exist in as-deposited CSSe thin films with stoichiometric formula Cd(SSe).

Quantitative analysis was carried out to confirm the atomic percentage of Cd, S and Se in as-deposited thin film using EDS pattern. Fig.5 indicates representative EDS spectrum of as-deposited $CSSe_4$ thin film. From Fig.5 it is observed that peaks at 3.13 KeV, 2.30 KeV and 1.38 KeV confirms presence of Cd, S and Se elements in as-deposited thin film respectively. Inset of Fig.5 shows tabulated data of expected and actual atomic percentage for Cd, S and Se elements. The small amount of digression of actual atomic percentage from expected atomic percentage of Cd, S, Se elements due to trace inclusion of oxygen in to the films from atmospheric contaminations and during transfer of films.[48,49] From table (inset of Fig.5) confirms actual atomic percentage of elements is in well agreement with expected atomic percentage.

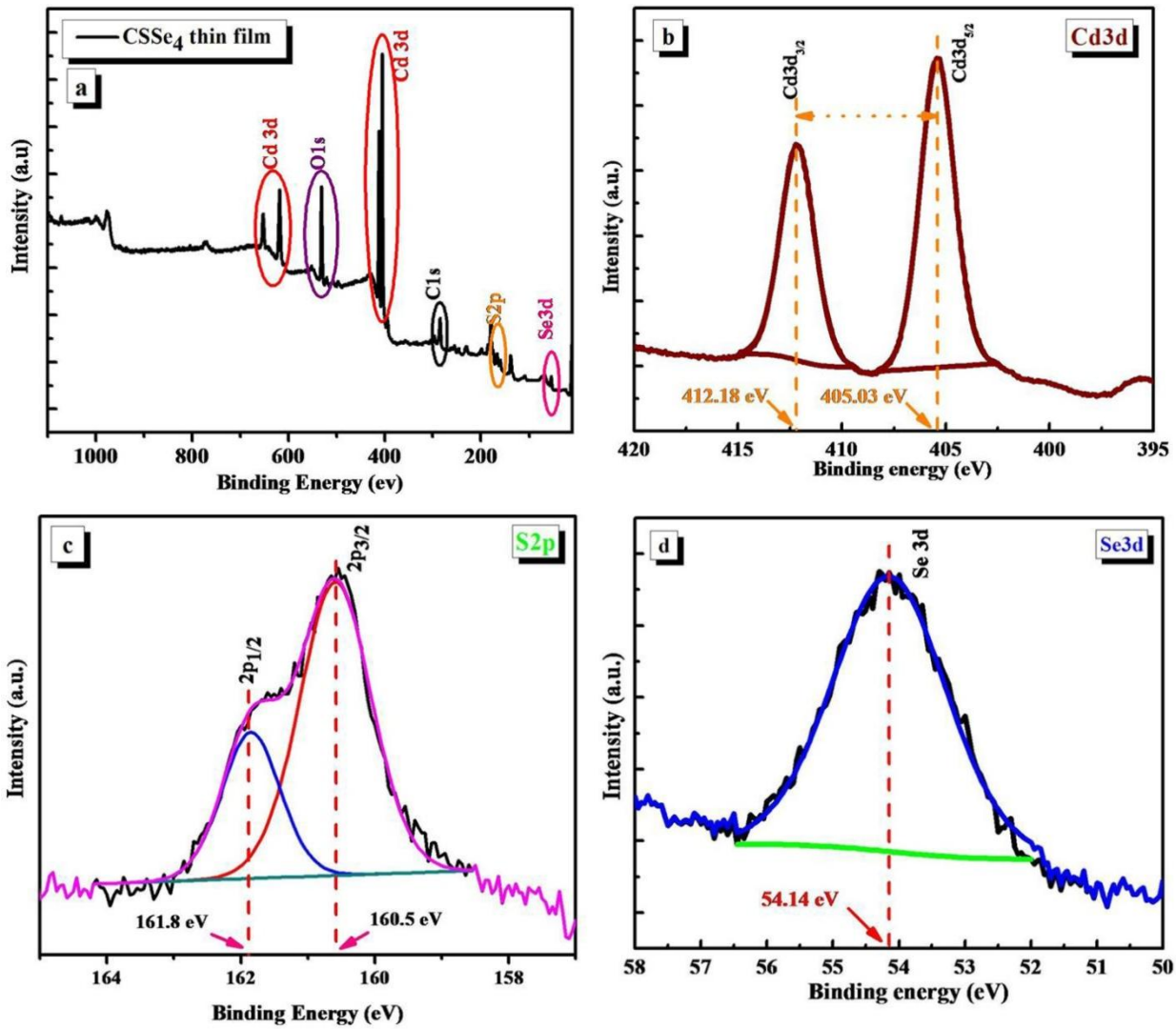

Fig. 4 (a) XPS survey spectrum of $CSSe_4$ thin film, **(b)** High resolution core level XPS spectrum of Cd, **(c)** High resolution core level XPS spectrum of S, **(d)** High resolution core level XPS spectrum of Se.

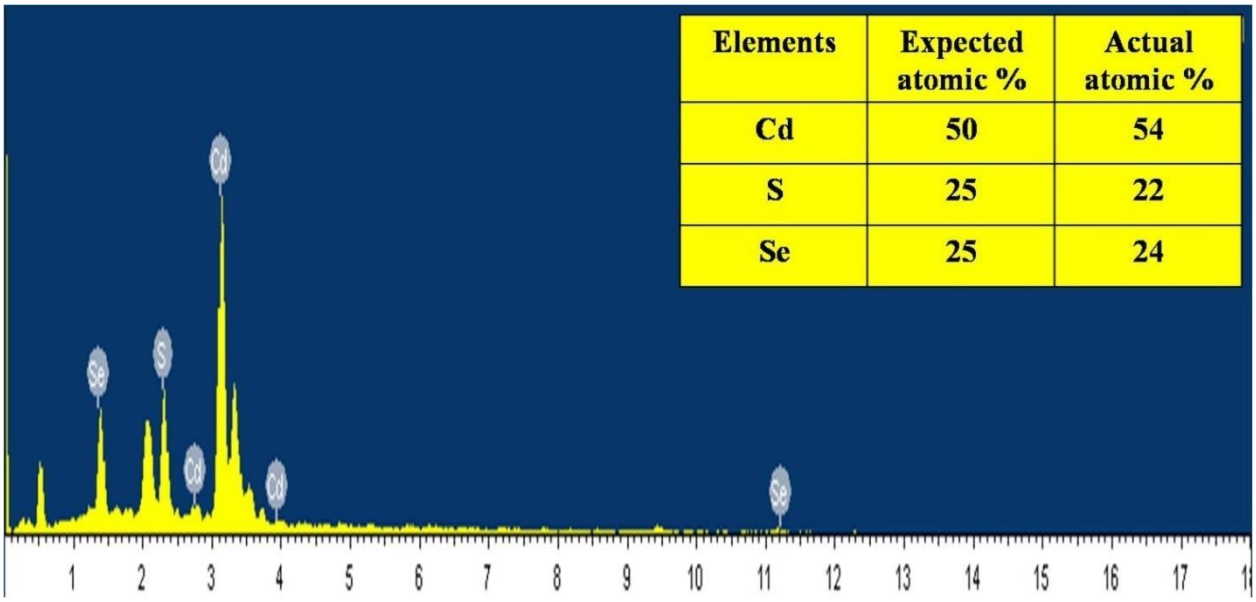

Elements	Expected atomic %	Actual atomic %
Cd	50	54
S	25	22
Se	25	24

Fig. 5 EDS spectrum of $CSSe_4$ thin film.

3.6 Electrical studies

Electrical conductivity is essential to study electrical transport properties of synthesized materials. Fig.6 shows plot of ln σ *vs* 1000/T for CSSe thin films with increase in deposition time. From plot (Fig.6) it is observed that with increase in deposition time conductivity increases for all samples. This increase in conductivity indicates CSSe thin films are semiconductor in nature. Activation energy was estimated by using equation 12 as follows,

$$\sigma = \sigma_0 e^{(-E_a/KT)} \qquad (12)$$

where σ is conductivity of sample, σ_0 is temperature independent part of conductivity, E_a is activation energy, k is Boltzmann constant, T is temperature in Kelvin. It is observed that activation energy decreases with increase in deposition time confirms high electrical conductivity of CSSe thin films.[23] Table 4 summarizes values of activation energy for CSSe thin films.

Thermoelectric power (TEP) measurement assesses difference between thermally generated voltage to temperature difference across hot and cold end of semiconducting material.[24] Plots of thermo *emf vs* temperature for CSSe thin films is shown in Fig.7. The negative polarity of generated thermo *emf* indicates all CSSe thin films are *n*-type semiconductor.[22,24] Carrier concentration and mobility for all samples were calculated by equations 13 and 14 as follows,

$$\log n = \left[\frac{3}{2}\log T - 0.005TEP + 15.719\right] \qquad (13)$$

$$\mu = \left[\frac{\sigma}{ne}\right] \qquad (14)$$

where, μ is mobility, n is carrier concentration and e is electronic charge. From Table 4, carrier concentration increase exponentially and mobility decreases with increase in deposition time. The increase in carrier concentration and decrease in mobility is might be due to low level of anti-structural defects present in deposited thin films.[22] The carrier concentration and mobility are specified in Table 4.

Table 4 Electrical properties of CSSe thin films.

Sr. No	Sample Code	Activation Energy (E_a, eV)	Carrier Concentration (n, 10^{19} cm^{-3})	Mobility 10^{-6} (μ,cm^{-2} V^{-1} S^{-1})
1	$CSSe_1$	0.064	3.455	1.850
2	$CSSe_2$	0.053	3.483	1.661
3	$CSSe_3$	0.044	3.517	1.592
4	$CSSe_4$	0.039	3.539	1.271

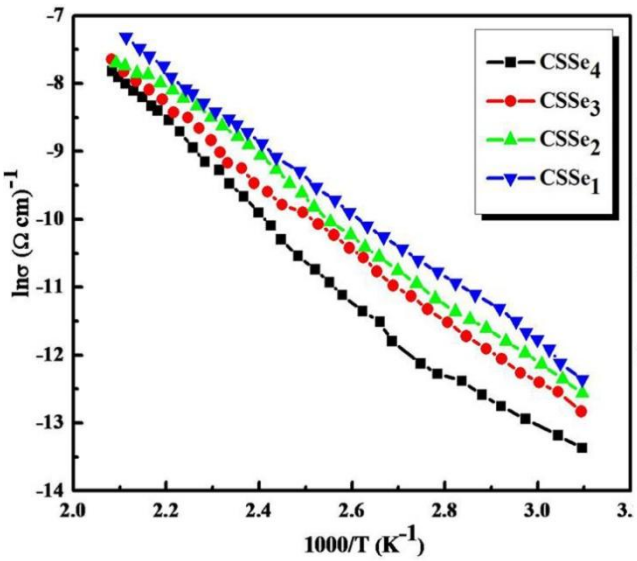

Fig. 6 Plots of ln σ vs 1000/T for CSSe thin films at various deposition time.

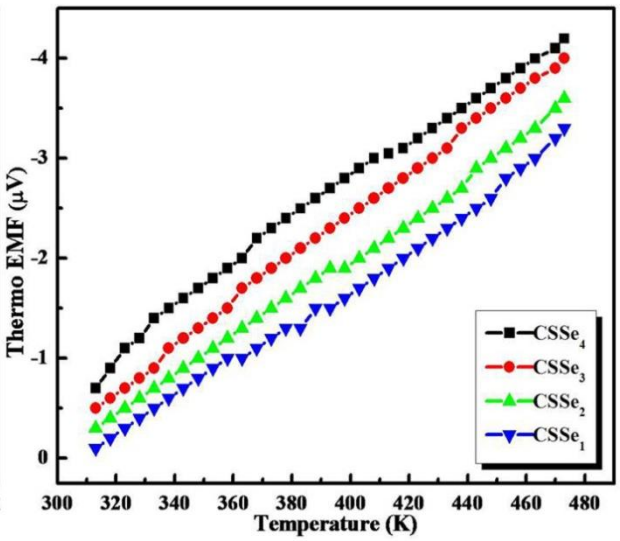

Fig. 7 Plots of thermo EMF vs temperature for CSSe thin films at various deposition time.

3.7 Photoelctrochemical (PEC) properties

PEC performance of all CSSe thin films was measured with standard two electrode configuration. Fig.8 show *J-V* curves of PEC cells formed by CSSe thin films as working electrode with active area 1 cm^2 and graphite (G) as counter electrode. All *J-V* measurements were done under illumination of light using 500 W tungsten filament lamp (Intensity 30 mW/cm^2) in 0.5 M sulfide/polysulfide redox electrolyte. In all samples, *J-V* characteristic in the dark shows ideal diode-like rectifying characteristics for PEC cells. Upon illumination, *J-V* curves were obtained in the fourth quadrant, indicating generation of electricity, which is distinctive PEC solar cell characteristics.[50] Also, for all CSSe thin films magnitude of photocurrent increase by way of negative polarity region demonstrating that material is *n*-type semiconductor,[51,52] This result is well consistent with observed TEP results. Photo response of all samples were conceded by forming subsequent cell configuration,

Glass-ITO/Cd(SSe)/polysulfide electrolyte, $(Na_2S\text{-}NaOH\text{-}S)_{aq.}$/G

Solar cell parameters such as, fill factor (FF), and conversion efficiency (η %) were calculated using relations (15) and (16) as follows,[53]

$$FF = \left(\frac{J_{\max} \times V_{\max}}{J_{sc} \times V_{oc}} \right) \qquad (15)$$

$$\eta(\%) = \left(\frac{J_{sc} \times V_{oc}}{P_{in}} \times FF \times 100 \right) \qquad (16)$$

where, J_{sc} is short-circuit current density and V_{oc} is open circuit voltage. J_{max} and V_{max} are maximum current density and maximum voltage, P_{in} is input light intensity (30 mW/cm^2). From *J-V* measurements, obtained values of J_{sc} for samples $CSSe_1$, $CSSe_2$, $CSSe_3$ and $CSSe_4$ were 0.247, 0.311, 0.366 and 0.454 mA/cm^2 and corresponding values of V_{oc} were 755, 758, 777 and 782 mV respectively. The values of series resistance (R_s) and shunt resistance (R_{sh}) of all samples were evaluated from the slope of power output characteristics using equations (17) and (18) as follows,[53]

$$\left[\frac{dI}{dV} \right]_{I=0} = \frac{1}{R_s} \qquad (17)$$

$$\left[\frac{dI}{dV} \right]_{V=0} = \frac{1}{R_{sh}} \qquad (18)$$

R_s varies from 429 Ω to 255 Ω for $CSSe_1$ to $CSSe_4$ thin films respectively. At same time, decrease in R_{sh} from 8103 Ω for $CSSe_1$ to 4189 Ω for $CSSe_4$ thin films is observed. R_s is based on resistance of metal contact, ohmic contact and junction depth where as R_{sh} is due to crystal defects. Ideally, R_s and R_{sh} should be 0 Ω and infinity respectively.[51] R_s, R_{sh}, FF and η (%) of all CSSe thin films are tabulated in Table 5.

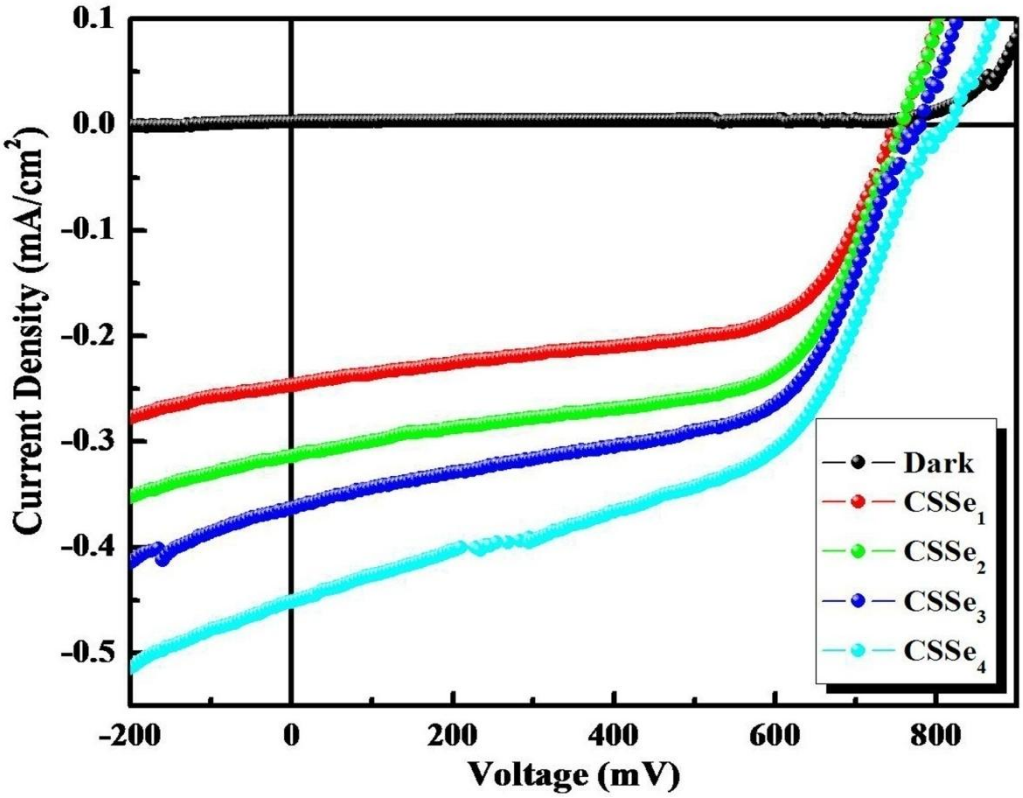

Fig. 8 *J-V* characteristics of CSSe thin films.

Table 5 Solar cell parameters of CSSe thin films.

Sample Code	E_g (eV)	J_{sc} (mA cm^{-2})	V_{oc} (mV)	J_{max} (mA cm^{-2})	V_{max} (mV)	R_s (Ω)	R_{sh} (Ω)	FF	η (%)
$CSSe_1$	2.01	0.247	755	0.187	581	429	8103	0.58	0.36
$CSSe_2$	1.95	0.311	758	0.245	553	329	6770	0.57	0.44
$CSSe_3$	1.90	0.366	777	0.278	560	276	4291	0.54	0.51
$CSSe_4$	1.86	0.454	782	0.319	536	255	4189	0.49	**0.57**

Highest conversion efficiency obtained was 0.57% for sample $CSSe_4$. From literature survey on Cd(SSe) thin films shows the obtained conversion efficiency is compatible with other reports on Cd(SSe) thin films deposited by highly sophisticated physical techniques.[10]

Good quality, highly adherent and densely packed CSSe thin films are favourable for absorption sufficient light radiations and generate photoelectrons. These generated photoelectrons transfer from nanocrystalline, pin-hole free and well adherent, compact layer to conducting substrate. Table 5 indicates that, boost in PEC performance for samples $CSSe_3$ and $CSSe_4$ compared to sample $CSSe_1$ and $CSSe_2$. This is because nanocoral-like surface morphology consists of interconnected a well grown nanocoral which increases surface area in contact with electrolyte. Also, samples $CSSe_3$ and $CSSe_4$ having better crystallinity, lower dislocation density and micro-strain respectively. This improved crystallinity is significantly reduces grain boundaries resistance. This reduced grain boundaries resistance effectively retards recombination of electron-hole pairs. As well as effective decrement in R_s for $CSSe_3$ and $CSSe_4$ thin films causes to enhancement in PEC performance. While that of $CSSe_1$ and $CSSe_2$ samples shows nanoflakes, assorted nanoflakes-nanospheres-like morphology, which has high dislocation density and micro-strain as compared to $CSSe_3$ and $CSSe_4$ thin films. As a result low conversion efficiency for $CSSe_1$ and $CSSe_2$ thin films is due to considerable grain boundaries in nanoflakes, assorted nanospheres-like morphology. Hence it is concluded that improvement in conversion efficiency of nanocoral-like morphology of CSSe thin films is due to crystalline nature of material, lower values of R_s, grain boundaries resistance

and decrease in dislocation density and micro-strain as compared to nanoflakes, assorted nanospheres-like morphology.

However, compared to other surface morphologies such as self-assembled nanoflower and micro-nano branch structures, obtained morphology (nanocoral-like) of Cd(SSe) thin films demonstrate low conversion efficiency may be due to,

1) Nubbly structured nanocoral-like surface morphology is containing limited surface area compared to other self-assembled nanoflower and micro-nano branch structured morphologies of Cd(SSe) thin film.

2) Naocoral-like morphology is closely packed by a variety of small grown nanosphere. But, on surface of nanocoral in between small nanosphere edges may contain some defect-induced surface states. These defects acts as trap for current carrier and results into to low conversion efficiency (0.57%) compared to other hierarchical morphologies.

From above, synthesis of CSSe thin films by APT is promising for development of solar cell devices. So, we are trying to deposit $Cd(S_{1-x}Se_x)$ thin films by varying bath composition and to engineer the novel surface morphology. Such morphologies may reduce defects-induced surface states. This surface states may reduces the surface traps for current carriers. These studies are underway in our laboratory.

4 Conclusions

In conclusion, we have first time reported facile, cost-effective, simple and hybrid APT method for deposition of nanocrystalline Cd(SSe) thin films using TEA as complexing agent. Opto-structural, morphological and photoelectrochemical studies concluded that TEA as complexing agent play crucial roles in growth process. Band gap energy is decreased from 2.01 to 1.86 eV with increase in thickness from 535-793 nm as function of deposition time respectively. XRD patterns of the as-deposited thin films illustrated that formation of nanocrystalline materials with pure hexagonal crystal structure. Crystallinity was improved with average crystallite size from 51 to 68 nm with decrease in dislocation density and micro-strain in CSSe thin films. The morphology changed from nanoflakes to assorted nanoflakes-nanospheres and finally nanocoral-like morphology with nearly stoichiometric CSSe thin films. Such morphology is beneficial for effective increase in photocurrent and efficiency of photoelectrochemical solar cell. All samples were semiconductor with *n*-type conductivity confirmed by EC and TEP measurements. Highest conversion efficiency obtained was 0.57% for $CSSe_4$ thin films. These might be due to low values of R_s and reduced grain boundaries resistance. These results promise the effective application of CSSe thin films that significantly helps for enhancement in light harvesting efficiency.

Acknowledgment

One of author KVK is very much thankful to Department of Science and Technology (DST), New Delhi for awarding DST-INSPIRE fellowship for financial assistance.

Notes and references

[a]*Materials Research Laboratory, Department of Chemistry, Shivaji University, Kolhapur, India.*

[b]*Polymer Energy Materials Laboratory, Advanced Chemical Engineering Department, Chonnam National University, Gwangju, South Korea.*

[c]*Thin film Materials Laboratory, Department of Physics, Shivaji University, Kolhapur, India.*

[d]*Photonic and Electronic Thin Film Laboratory, Department of Materials Science and Engineering, Chonnam National University, Gwangju, South Korea.*

[e]*Department of Materials Science and Engineering and Optoelectronics Convergence Research Center, Chonnam National University, Gwangju, South Korea.*

E-mail address: p_n_bhosale@rediffmail.com

Tel Number: 091-231-2609338, Fax: +91-231-2691533, 2692333 (O).

1 G. Chen, J. Seo, C. Yang, P. N. Prasad, *Chem. Soc. Rev*.,2013,**42**, 8304.
2 S. S. Mali, H. Kim, C. Shim, P. S. Patil, J. H. Kim, C. K. Hong, *Sci. Rep.*, 2013, **3**, 3004.
3 S. G. Kumar and K. S. R. K. Rao, *Energy Environ. Sci*., 2014, **7**, 45.
4 M. Yuan and D. B. Mitzi, *Dalton Trans.*, 2009, 6078.
5 P. Mandal, R.S. Srinivasa, S.S. Talwar, S.S. Major, *Appl. Surf. Sci.*, 2008, **254**, 5028.
6 V. Kumar, S. K. Sharma, D. K. Dwivedi, *J. Alloys Compd*., 2012, **512**, 351.
7 T. Gruszecki, B. Holmstorm, *Sol. Energy Mater. Sol. Cells*., 1993, **31**, 227.
8 J. Heo, H. Ahn, R. Lee, Y. Han, D. Kim, *Sol. Energy Mater. Sol. Cells.*, 2003, **75**, 193.
9 C. J. Hibberd, K. Ernits, M. Kaelin, U. Muller, A.N. Tiwari, *Prog. Photovolt: Res. Appl.*,2008, **16**, 585.
10 A. A. Yadav, E. U. Masumdar, *Solar Energy.*, 2010, **84**, 1445.
11 S. D. Chavhan, R. S. Mane, T. Ganesh, L. Wonjoo, S.H. Han, S. Senthilarasu, S. H. Lee, *J. Alloys Compd*., 2009, **210**, 474.
12 F. Liu, Y. Lai, J. Liu, B. Wang, S. Kuang, Z. Zhang, J. Li, Y. Liu, *J. Alloys Compd*., 2010, **305**, 493.
13 J. B. Chaudhari, N. G. Deshpande, Y. G. Gudage, A. Ghosh, V. B. Huse, R. Sharma, *Appl. Surf. Sci.*, 2008, **254**, 6810.
14 D. S. Reddy, K. N. Rao, K. R. Gunasekhar, Y. D. Reddy, P. S. Reddy, *J. Alloys Compd*., 2008, **34**, 461.
15 E. Bacaksiz, S. Aksu, I. Polat, S. Yılmaz, M. Altunbas¸ *J. Alloys Compd.*, 2009, **280**, 487.
16 D. P. Padiyan, A. Marikani, K.R. Murali, *J. Alloys Compd.* 2004, **8**, 365.
17 K. Prabakar, S. K. Narayandass, D. Mangalaraj, *J. Alloys Compd*., 2004, **64**, 233.
18 Y. Liu, Y. Xu, J. P. Li, B. Zhang, D. Wu, Y. H. Sun, *Mater. Res. Bull.*, 2006, **99**, 41.
19 K. P. Bhuvana, J. Elanchezhiyan, N. Gopalakrishnan, T. Balasubramanian, *J. Alloys Compd.*, 2009, **473**, 534.
20 A. A. Yadav, M. A. Barote, E. U. Masumdar, *Mater. Chem. Phys.*, 2010, **53**, 121.
21 R. M. Mane, S. R. Mane, R.R. Kharade, P.N. Bhosale, *J. Alloys Compd*., 2011, **491**, 321.
22 N. B. Pawar, S. S. Mali, S. D. Kharade, M. G. Gang, P.S. Patil, J. H. Kim, C. K. Hong, P. N. Bhosale, *Curr. Appl. Phys.*, 2014, **14**, 508.
23 S. V. Patil, R. M. Mane, N. B. Pawar, S. D. Kharade, S. S. Mali, P. S. Patil, G. L. Agawane, J. H. Kim, P. N. Bhosale, *J Mater Sci: Mater Electron.*, 2013, **24**, 4669.

24 M. M. Salunkhe, R. R. Kharade, S. D. Kharade, S. S. Mali, P. S. Patil and P. N. Bhosale, *Mater. Res. Bull*., 2012, **47**, 3860.
25 G. Li, Y. Jiang, Y. Wang, C. Wang, Y. Sheng, J. Jie, J. A. Zapien, W. Zhang and S. Lee, *J.* Phys. Chem. C., 2009,**113**, 17183.
26 H. Liu, J. Lu, M. Zheng, S. Hai Tang, X. Zhang and C. H. Sow, *Nano Research*., 2013, **6(11)**, 808.
27 B. D. Ajalkar, R. K. Mane, B. D. Sarwade, P. N. Bhosale, *Sol. Energy Mater. Sol. Cells.*, 2004, **81**, 101.
28 A. R. Patil, V. N. Patil, P. N. Bhosale, L. P. Deshmukh, *Mater. Chem. Phy.*, 2000, **65**, 266.
29 B. D. Ajalkar, R. K. Mane, P. N. Bhosale, *J. Mater. Sci*., 2003, **39**, 1657.
30 R. M. Mane, P. N. Bhosale, Synthesis & Characterization of Mixed Metal Chalcogenide Thin Films, *Lambert Academic Publications (LAP)*, 2013.
31 S. H. Pawar, P.N. Bhosale, *Mater. Chem. Phys*. 1984, **11**, 461.
32 W. Ostwald, Lehrbuch der Allgemeinen Chemie, Leipzig, Germany, 1896, **2(1)**.
33 S. S. Mali, P. S. Patil, and C. K. Hong, *ACS Appl. Mater. Interfaces.*, 2014, **6**, 1688.
34 J. Pelleg, E. Elish, *J. Vac. Sci. Technol.A.*, 2002, **20**, 754.
35 J. Reddy, M.K. Kokila, H. Nagabhushan, R.P.S. Chakradhar, C. Shivakumar, J.L. Rao, B.M. Nagabhushan, *J. Alloys. Compd*., 2011, **509**, 5349.
36 R. Herberholz, M.J. Carter, *Sol. Energy Mater. Sol. Cells.*, 1996, **44**, 357.
37 B.D. Cullity, The Elements of X-ray Diffraction, 1st edn, *Add1son-Wesley Publishing* Company Inc., USA., 1957.
38 S. Min, O. Joo, R.S. Mane, K. Jung, C.D. Lokhande, S. Han, *Photochem. Photobiol. A*., 2007, **187,** 133.
39 R., P. Prathap, R.W. Miles, K.T. Ramakrishna Reddy, *Sol. Energy Mater. Sol. Cells.*, 2010, **94,** 1487.
40 T. Kameyama, T. Osaki, K. Okazaki, T. Shibayama, A. Kudo, S. Kuwabatade, T. Torimoto, *J. Mater. Chem.*, 2010, **20,** 5319.
41 K. V. Khot, S. S. Mali, N. B. Pawar, R. M. Mane, V. V. Kondalkar, V. B. Ghanwat, P. S. Patil, C. K. Hong, J. H. Kim, J. Heo P. N. Bhosale, *J Mater Sci: Mater Electron*., 2014, **25,** 3762.
42 U. Pal, D. Samantha, S. Ghorai, A.K. Chaudhuri, *J. Appl. Phys.*, 1993, **74**, 6368.
43 V. Bilgin, S. Kose, F. Atay, I. Akyur, *Mater. Chem. Phys.*, 2005, **94**, 103.
44 V. M. Garcia, M. T. S. Nair, P. K. Nair, R. A. Zingaro, *Semicond. Sci. Technol*., 1997, **12,** 645.
45 S. F. Ahmed, S. Khan, P. K. Ghosh, M. K. Mitra, K. K. Chattopadhyay, *Sol–Gel Sci. Technol*,. 2006, **39**, 214.
46 S. S. Mali, P. S. Shinde, C. A. Betty, P. N. Bhosale, W. J. Lee and P. S. Patil, *Prog. Photovolt: Res. Appl*,. 2014, **22,** 525.
47 M. Muthusamy and S. Muthukumaran, *J Mater Sci: Mater Electron.*, 2013, **24,** 2277.
48 J. Horak, K. Cermark, L. Koudelkar, *J. Phys. Chem. Sol*., 1886, **47,** 805.
49 L. J. Horak, L. Koudelkar, *J. Phys. Stat. Sol. A.*, 1984, **84,** 143.
50 S. A. Vanalakar, S. S. Mali, R. C. Pawar, N. L. Tarwal, A. V. Moholkar, J. A. Kim, Ye-bin Kwon, J.H. Kim, P.S. Patil, *Electrochim Acta*., 2011, **56,** 2762.
51 C. Garza, S. Shaji, A. Arato, E. P. Tijerina, G. A. Castillo, T. K. Das Roy, B. Krishnan, *Sol Energy Mater Sol Cells*, 2011, **95**, 2001.
52 S. B. Ambade, R. S. Mane, S. S. Kale, S. H. Sonawane, A. V. Shaikh, S. H. Han, *Appl Surf Sci.*, 2006, 253.
53 S. S. Mali, B. M. Patil, C. A. Betty, P. N. Bhosale, Y. W. Oh, S. R. Jadkar, R. S. Devan, Y. R. Ma, P. S. Patil, *Electrochim Acta.*, 2012, **66**, 216.